Mon. Not. R. Astron. Soc. **377,** 507–515 (2007) doi:10.1111/j.1365-2966.2007.11637.x

The radial Tully–Fisher relation for spiral galaxies – I

Irina A. Yegorova★ and Paolo Salucci

SISSA – International School for Advanced Studies, via Beirut 2-4, Trieste, Italy

Accepted 2007 February 16. Received 2007 January 31; in original form 2006 May 22

ABSTRACT

We find a new Tully–Fisher-like relation for spiral galaxies holding at different galactocentric radii. This radial Tully–Fisher relation allows us to investigate the distribution of matter in the optical regions of spiral galaxies. This relation, applied to three different samples of rotation curves of spiral galaxies, directly proves that: (i) the rotation velocity of spirals is a good measure of their gravitational potential and both the rotation curve's amplitudes and profiles are well predicted by galaxy luminosity, (ii) the existence of a dark component, less concentrated than the luminous one, and (iii) a scaling law, according to which, inside the disc optical size: $M_{\rm dark}/M_{\rm lum} = 0.5(L_B/10^{11}\,{\rm L}_{B\odot})^{-0.7}$.

Key words: galaxies: kinematics and dynamics – galaxies: spiral – dark matter.

1 INTRODUCTION

Tully & Fisher (1977) discovered that the maximal rotational velocity $V_{\rm max}$ of a spiral galaxy, measured by the full width at half-maximum (FWHM) of the neutral hydrogen 21-cm line profile, correlates with the galaxy luminosity by means of a power law of exponent $a \sim 4$. This equivalently reads as

$$M = a \log V_{\rm max} + b, \tag{1}$$

with M being the absolute magnitude in some specified band and b being a constant. It was immediately realized that this relation, hereafter TF, could serve as a powerful tool to determine the distances of galaxies (Pierce & Tully 1988) and to study their dynamics (Persic & Salucci 1988). The rotational velocity reflects the equilibrium configuration of the underlying galaxy gravitational potential, especially when $V_{\rm max}$ is directly derived from extended rotation curves (RCs). Before proceeding further, let us point out that spiral galaxies have a characteristic size scale, $R_{\rm opt}$, that sets also a characteristic reference velocity $V(R_{\rm opt})$. $R_{\rm D}$, the exponential thin disc length-scale, is a natural choice for such reference radius; in this paper, however, we adopt for the latter a minimal variant, i.e. a multiple of this quantity: $R_{\rm opt} \equiv 3.2R_{\rm D}$ (see Persic, Salucci & Stel 1996, hereafter PSS). (No result here depends on the value of the multiplicity constant.) This choice is motivated by the fact that 3.2 $R_{\rm D}$, by enclosing 83 per cent of the total light, is a good measure of the 'physical size' of the stellar disc, and that, for many purposes, $V_{\rm opt} \equiv V(R_{\rm opt}) = V_{\rm max}$.[1]

Let us stress that some known kinematical quantities are not suitable reference velocities. For example, the value of $V_{\rm max}$ for a spiral depends on the extension and on the spatial resolution of the available RC and, in addition, it does not have a clear physical interpretation, sometimes coinciding with the outermost available velocity measure, in other cases with the innermost one. Also $V_{\rm last}$, the velocity at the outermost measured point, obviously does not have a proper physical meaning, in addition some spirals never reach the, so-called, asymptotic flat regime (PSS and Salucci & Gentile 2006).

Coming back to the TF relation, its physical explanation, still not fully understood, very likely involves the argument that in self-gravitating rotating discs both the rotation velocity and the total luminosity are a measure of the same gravitational mass (e.g. Strauss & Willick 1995). Note that, if this argument is correct, both $V_{\rm max}$ and $V_{\rm last}$ are just empirical quantities of different and not immediate physical meaning.

The existence of the TF can be understood as it follows. The stars in spiral galaxies are essentially settled in thin discs with an exponential surface mass distribution (Freeman 1970)

$$\Sigma(R) = \Sigma_0 {\rm e}^{-R/R_{\rm D}}, \quad \Sigma_0 = k_1 L^s, \tag{2}$$

where k_1 and s are constants, $\Sigma_0 = (M_{\rm d}/L)\, I_0$ is the central surface mass density with I_0 being the central surface brightness, that in the first approximation, can be set constant among spirals. L and $M_{\rm D}$ are the total luminosity in a specific band and the disc mass. Since from equation (2), $M_{\rm D} \propto \Sigma_0 R_{\rm D}^2$, the above approximation implies that $R_{\rm D} \propto L^{0.5}$. Let us now consider the condition of self-gravity equilibrium for the stellar disc, i.e. the ratio $E = GM_{\rm D}/(V_{\rm opt}^2 R_{\rm opt})$. By writing

$$E = k_2 L^t, \tag{3}$$

where k_2 and t are constants, we have that Freeman discs are completely self-gravitating for $k_2 \simeq 1.1$ and $t = 0$. By setting $s = 0$, i.e. by assuming that the disc mass-to-light ratios are constant among spirals, we arrive to the well-known relation: luminosity $\propto$ (velocity)^4. Random departures from the above conditions induce a larger scatter in the TF relation, while systematic departures,

★E-mail: yegorova@sissa.it

[1] For the Persic & Salucci (1995) (hereafter PS95) sample, $\log V_{\rm opt} = (0.08 \pm 0.01) + (0.97 \pm 0.006) \log V_{\rm max}$.

e.g. variations of the stellar population with galaxy luminosity or violation of the condition of self-gravity, modify slope, zero-point and scatter, possibly in a band-dependent way. More generally we can write $L \propto V_{\rm opt}^{2/(s+0.5-t)}$ (here s and t can be band-dependent), while we can also envisage a more complex and perhaps non-linear relationship, if the above scaling laws are not just power laws and I_0 varies among galaxies. From an observational point of view, by studying several large samples of galaxies, it has been found that the TF has different slope and scatter in different bands: $a_I \simeq 10$, $s_I \sim 0.4$ mag, while $a_B \simeq 7.7$, $s_B \sim 0.5$ mag (e.g. Pierce & Tully 1992; Salucci, Frenk & Persic 1993). Furthermore, a non-linearity in the TF is often found at low rotation velocities (Aaronson et al. 1982).

We know that spiral galaxies are discs of stars embedded in (almost) spherical haloes of dark matter (DM) and this is crucial for understanding the physical origin of the TF relation (Persic & Salucci 1988; Strauss & Willick 1995; Rhee 1996). It is well known that the dark haloes paradigm is supported by the (complex) mass modelling of galactic RCs (e.g. PSS and references therein) and it implies that discs are not fully self-gravitating. At any radius, both the dark and luminous components contribute to the (observed) rotational velocity $V(R)$, with a relative weight that varies both radially and from galaxy to galaxy. The resulting model circular velocity can be written as a function of the useful radial coordinate $x \equiv R/R_{\rm opt}$ as[2]

$$V_{\rm model}(x) = (GM_{\rm D}/R_{\rm D})^{1/2}\,[f_{\rm d}(x)/f_{\rm d}(1) + \Gamma\, f_{\rm h}(x,\alpha)]^{1/2}, \qquad (4)$$

where $f_{\rm d}(x)$ is the Freeman velocity disc profile

$$f_{\rm d}(x) = \frac{1}{2}(3.2x)^2[I_0(1.6x)K_0(1.6x) - I_1(1.6x)K_1(1.6x)], \qquad (5)$$

and

$$f_{\rm h}(x,\alpha) = \left(\frac{x^2}{x^2+\alpha^2}\right)(1+\alpha^2), \qquad (6)$$

$M_{\rm D}$ is the disc mass, Γ is the dark/visible matter velocity ratio at $R_{\rm opt}$ and α is the halo velocity core radius in units of $R_{\rm opt}$. The adopted halo function $f_{\rm h}(x,\,\alpha)$ (see PSS) is the simplest way to describe, inside the optical radius, the contribution of DM halo; in fact, for an appropriate value of the parameter α, in $V_{\rm model}(x)$, it describes both the 'empirical' universal rotation curve (URC) halo velocity profile in PSS and (by setting $\alpha = 1/3$) the N-body Lambda cold dark matter (Λ CDM) $V_{\rm NFW}(x)$ Navarro–Frenk–White halo velocity profile.

Let us point out that, given the existence of the TF relation ($L \propto V_{\rm opt}^k$, k = constant), with the circular velocity described by equation (4), any dependence on luminosity of the mass distribution parameters Γ and α triggers, at radii $jR_{\rm opt}(j = 0.2$–$1.4)$, a whole family of relationships, similar to the TF one, but with slopes, scatters and zero-points all different and all depending on the detailed characteristics of the mass distribution.

We show this in Fig. 1 where, from the *empirical* (TF) relation

$$L_B = \left(\frac{V_{\rm opt}}{200\,{\rm km\,s^{-1}}}\right)^{3.5} 10^{11}\,{\rm L}_{B\odot}, \qquad (7)$$

holding at $R_{\rm opt}$ we predict the new relation that holds at an inner radius according to specific mass models. Among those, it is worth discussing in detail for the model that underlies the URC: i.e. $\Gamma = 0.5\ (L_B/2.5\times 10^{10}{}_{\odot}{}^{0.2})^{-0.9}$; $\alpha = 1.5\ (L_B/5\times 10^{10}{}_{\odot})^{0.2}$. In this case, the predicted slope decreases from 3.5 at $R_{\rm opt}$ to 2.75 at $0.6R_{\rm opt}$ and to 2.5 at $0.4R_{\rm opt}$. If the above is considered just as a toy model obviously the predicted slopes do not carry any uncertainties, if, instead, it is considered as the URC mass model, they carry a 15 per cent uncertainty due propagation errors from Γ and α.

[2] For simplicity here we neglect the bulge, we will consider it in Section 4.

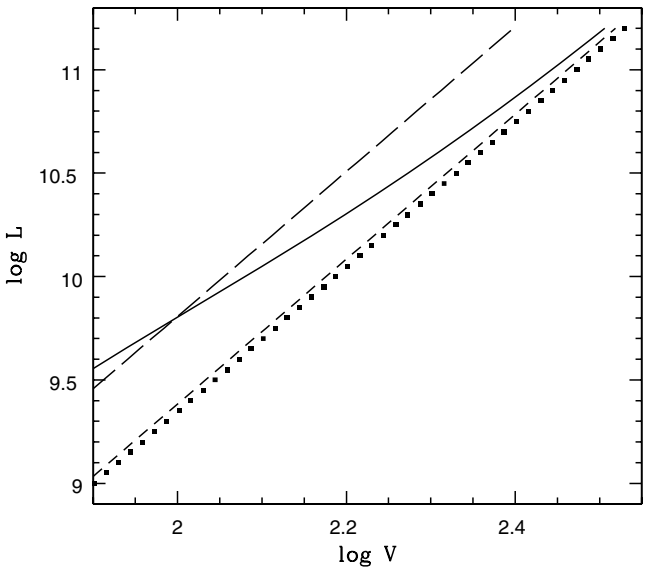

Figure 1. The TF relation at $R_{\rm opt}$ (triangles) and the predicted relation at 0.6 $R_{\rm opt}$ in the cases of no-DM (short dashed line), $\Gamma = 1$ NFW halo (long dashed line), the URC mass model (see the text, solid line).

Therefore the URC paradigm implies, in addition to a universal velocity profile at any chosen luminosity, also a 'TF-like' relationship at any chosen radius $JR_{\rm opt}$, whose actual characteristics, however, are not investigated in PSS, and are not easy to recover from the underlying mass model.

This will be instead easily done in the present paper, meant to be complementary to PSS; we will come back to the RCs to directly investigate them extracting from actual data the radial Tully–Fisher (RTF) relation, i.e. a family of TF-like relations holding at any properly chosen radial distance. To ensure a better statistical coverage, this will be repeated for three samples of spirals with different selection criteria and reference luminosity bands. These samples mostly contain Sb–Sc spiral galaxies with the number of early-type spirals and dwarfs being very small. Moreover, in general, the bulge affects only the first reference radius. Different investigations will be necessary to assess the present results in bulge-dominated spirals and H I-dominated dwarfs.

Finally, we will use the properties of such relationships to investigate the mass distribution in late-type spirals.

The plan of this work is the following. In Section 2, we describe our data samples and the main steps of the analysis. In Section 3, we show that TF-like relations hold at specific radii, and we derive the basic parameters of these relations for our samples. In the next section, we discuss the implications of the existence of RTF relation and we propose a simple mass model (SMM) that fits the data. The conclusions are given in Section 5.

2 DATA AND ANALYSIS

Sample 1 consists of 794 original RCs of PS95 (note that for most of them the limited number of independent measurements and sometimes some non-circular motion make it difficult to derive a proper

mass model, but instead this can be done with the method in Sections 2 and 3).

In each RC, the data are radially binned on a $0.2R_{\rm opt}$ scale so that we have 4–7 independent and reliable estimates of the circular velocity, according to its extension.

Sample 2 from Courteau (1997) consists of 86 RCs (selected from 304 galaxies), and Sample 3 of Vogt et al. (2004) consists of 81 RCs (selected from 329 galaxies). These samples have been built by selecting from the original samples only objects with high quality and high-resolution kinematics yielding reliable determinations of both *amplitudes* and *profiles* of the RCs. To ensure this, we have set the following selection criteria. The RCs must (i) extend out to $\simeq R_{\rm opt}$, (ii) have at least 30 velocity measurements distributed homogeneously with radius and between the two arms and (iii) show no global asymmetries or significant non-circular motions; the profiles of the approaching and receding arms must not disagree systematically more than 15 per cent over $1R_{\rm d}$ length-scale. The velocity errors are between 1 and 3 per cent.

In each galaxy, we measure the distance from its centre R in units of $R_{\rm opt}(R_{\rm opt} \equiv 3.2R_{\rm D})$ and we consider a number of radial bins centred at $R_{\rm n} = (n/5)R_{\rm opt}$ for the PS95 sample and at $R_{\rm n} = (n/20)R_{\rm opt}$ for the other two samples; we take the bin size $\delta = 0.2R_{\rm opt}$ for the PS95 sample and $\delta = 0.06R_{\rm opt}$ for the other two samples. Then we co-add and average the velocity values that fall in the bins, i.e. in the radial ranges $R_{\rm n} - \delta/2 \leqslant R_{\rm n} \leqslant R_{\rm n} + \delta/2$ and we get the average circular velocity $V_{\rm n}$ at the chosen reference radii $R_{\rm n}$. (For the PS95 sample this was made in the original paper.)

A 'large' radial bin size has been chosen for the (much bigger) PS95 sample because, by selection, most of its RCs have a relatively smaller number of measurements. For the other two samples, that exclusively includes extended high-quality RC and large number of measurements we decrease the bin size by a factor of 3.2.

In short, we will use two different kinds of samples: Sample 1 includes 794 Sb–Sd galaxies with *I* magnitudes whose RCs are estimated inside large radial bins that smooth out non-circular motions and observational errors; Samples 2 and 3 include 167 galaxies with *R* magnitudes, whose RCs of higher quality are estimated inside smaller radial bins providing so a larger number of independent data per object.

We look for a series of correlations, at the radii $R_{\rm n}$ between the absolute magnitude M (in bands indicated below) and $\log V_{\rm n} \equiv \log V(R_{\rm n})$. Data in the *I* (Mathewson, Ford & Buchhorn 1992a) and *r* (Courteau 1996; Vogt et al. 2004a) bands will allow us to check the dependence of our results on the type of stellar populations in spiral galaxies. Finally, let us stress that the uncertainties of photometry are about 10 per cent and therefore negligible.

3 THE RTF RELATIONSHIP

Given a sample of galaxies of magnitude $M_{\rm band}$ and reliable rotational curves, the RTF relation is defined as the ensemble of the fitting relationships

$$M_{\rm band} = a_{\rm n} \log V_{\rm n} + b_{\rm n}, \tag{8}$$

with $a_{\rm n}$ and $b_{\rm n}$ being the parameters of the fits and $R_{\rm n}$ being the radial coordinates at which the relationship is searched. The latter is defined for all objects as a fixed multiple of the disc length-scale (or equivalently a multiple of $R_{\rm opt}$). Parameters $a_{\rm n}$ and $b_{\rm n}$ are estimated by the least-squares method (without considering the velocity/magnitude uncertainties).

The existence of the RTF relation is clearly seen in Figs 2 and 3, where all the TF-like relations for the PS95 sample are plotted together and identified with a different colour. It is immediate to realize that they mark an ensemble of linear relations whose slopes and zero-points vary continuously with the reference radius $R_{\rm n}$.

Independent Tully–Fisher-like relationships exist in spirals at any 'normalized' radius $R_{\rm n}$. We confirm this in a very detailed and quantitative way in Figs A1 and A2 and in Tables A1–A3, where very similar results are found for the other two samples. It is notable that the various investigations lead to the same consistent picture.

The slope $a_{\rm n}$ increases monotonically with $R_{\rm n}$; the scatter $s_{\rm n}$ has a minimum at about two disc length-scales, $0.6\ R_{\rm opt}$. In the *I* band, the values of the slopes are about 15 per cent larger than those in the *r* band. This difference, well known also for the standard TF, can be interpreted as due to the decrease, from the *r* to the *I* band, of the parameter *s* (see equation 2), as an effect of a different importance in the luminosity of the population of recently formed stars (Strauss & Willick 1995).

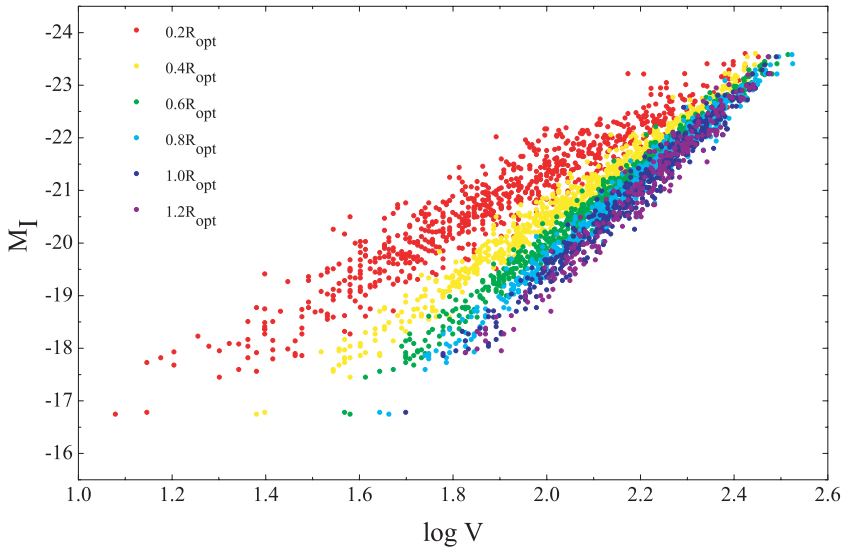

Figure 2. The RTF relations for the PS95 sample. Each one of the six relations is indicated with different colours.

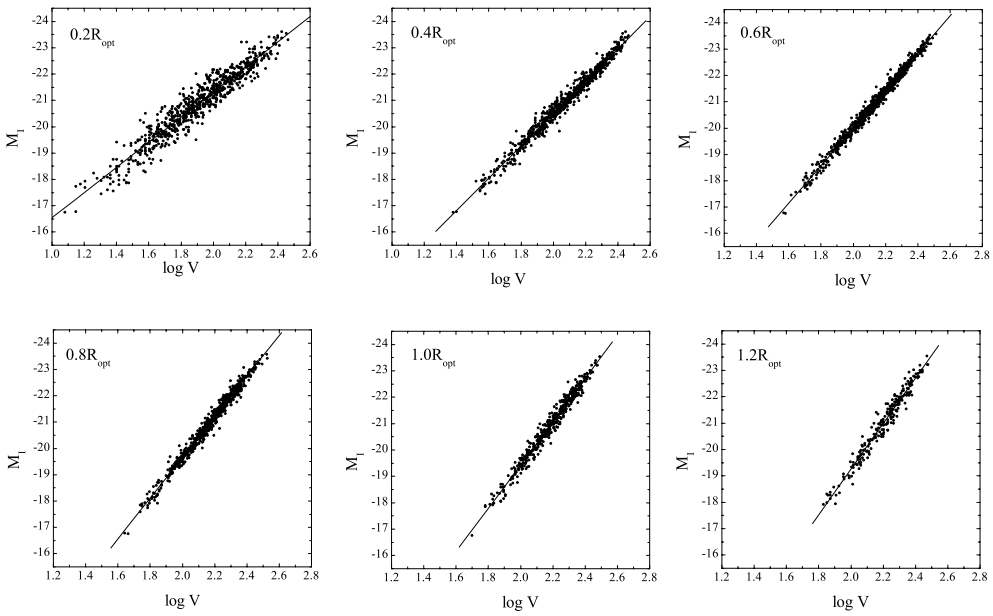

Figure 3. The RTF relation for the PS95 sample.

It is possible to compare the RTF relations in different bands; in the case of the absence of DM, true in the inner regions of spirals (except in the very luminous galaxies and low surface brightness almost absent in our sample), for the reasonable values $s_r = 0.1$ and $s_I = 0$ the power-law coefficient of the L_I versus velocity relationship is larger by a factor of $(0.5 + s_r)/(0.5 + s_I)$ than that of the L_r versus velocity relationship, in details by a factor of 1.2. This correction allows us to compare the a_n slopes as a function of R_n for our samples (see Fig. 4). Remarkably, we find that the values of the slopes vary with R_n according to a specific pattern:

$$b_n = -2.3 - 9.9(R_n/R_{opt}) + 3.9(R_n/R_{opt})^2. \quad (9)$$

It is worth looking at the scatter of the RTF relation (see Fig. 5). We find that, near the galactic centre, the scatter is large 0.3–0.4 dex, possibly due to a 'random' bulge component governing the local kinematics in this region being almost independent of the total galaxy magnitude. The scatter starts to *decrease* with R_n, to reach a minimum of 0.15–0.3 dex at R_n corresponding to two disc length-scales, the radius where the contribution of the disc to the circular velocity $V(R)$ reaches the maximum. From $2R_D$ onwards, the scatter increases outwards reaching 0.3 dex, at the farthest distances with available data, i.e. at 3–4 disc length-scales.

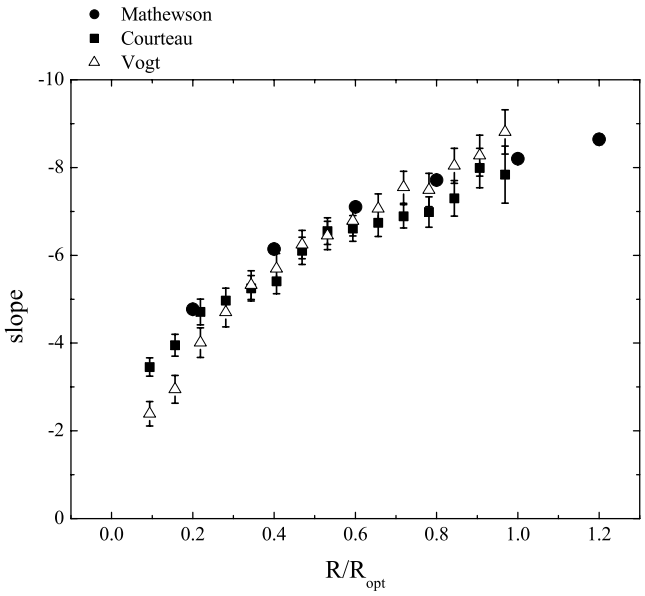

Figure 4. The slope of the RTF relation at different radii for the three samples. The slope for the standard TF is about to −7.5.

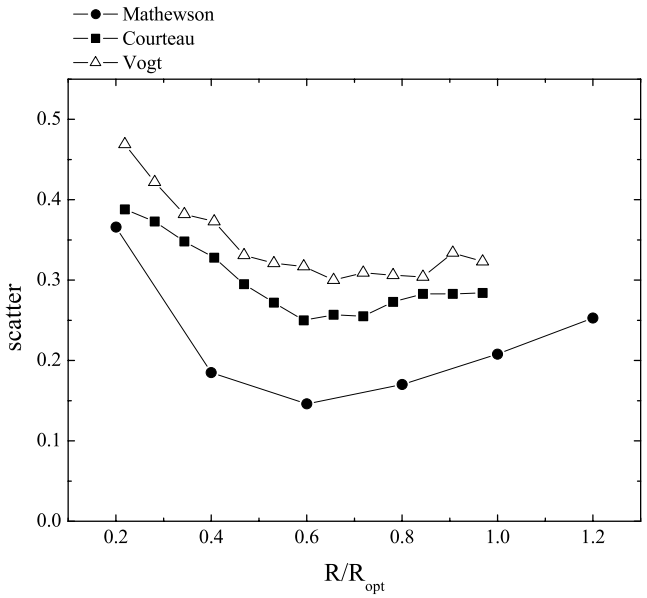

Figure 5. The scatter of the RTF relation at different radii for the three samples.

Let us note that these scatters are remarkably small. Most of the relations in the RTF family are statistically at least as significant as the standard TF relation, while the most correlated ones show a scatter of only 0.2–0.3 mag (i.e. significantly smaller than that of the standard TF; see Fig. 7). Since they include also the effects of

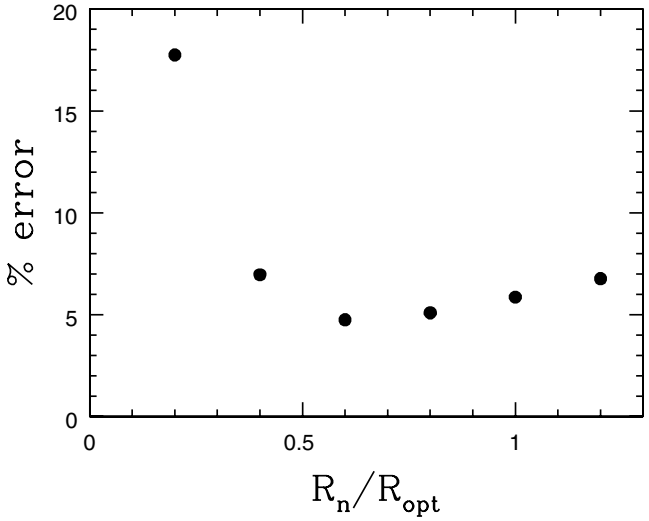

Figure 6. The per cent errors of the rotational velocity for different radii.

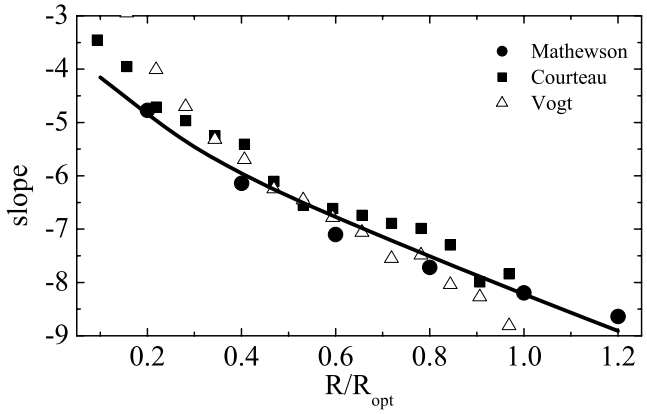

Figure 8. Slopes a_n of the RTF relation for the three samples as a function of the reference radius in units of R_{opt}. The solid line is the best-fitting relation for equation (14).

various observational errors, their small values could indicate that there is a very small intrinsic scatter in the RTF relation.

An important consequence of the smallness of the scatter of TF-like relationships is that it allows us to claim that, at any radius x, the luminosity empirically *predicts* the rotation velocity of spirals within the very small error of

$$\delta V_n/V_n = \ln(10)s_n/a_n \quad (10)$$

that, using the data from Tables A1–A3, is found to range between 5 and 7 per cent for the PS95 sample and between 10 and 12 per cent for the other two samples (see Fig. 6). Even in the very inner bulge-dominated regions (not studied here and in PSS), it does not exceed 20 per cent. The smallness of $\delta V_n/V_n$ is remarkable also because this quantity includes distance and inclination errors so as a contribution from non-circular motions, that in principle should be removed from the estimate of the 'prediction error', intrinsic to the RTF. The fact that the latter relationship is able to reproduce the rotation velocities of spirals within few per cent, it is a proof for the URC paradigm, additional and perhaps more impressive than the small rms of the set of synthetic RCs in PSS.

Incidentally, the existence of a radius ($x = 0.6$) at which the TF-like relations show a minimum in the internal scatter (much less pronounced in the prediction error $\delta V_n/V_n$) is not related to the overall capability of the luminosity to 'measure' the rotation velocities. In fact, at very small x the (random) presence of a bulge increases the scatter of the TF-like relation, in that, at these radii, the actual kinematical-photometric Fundamental Plane includes (as in ellipticals) a third quantity (the central brightness). At large x, the modest increase of the scatter is likely due to an increase of observational errors.

The scatter of the RTF in the R band for the corresponding samples is somewhat larger than that in the I band for the PS95 sample. This can be easily explained by the following: (i) the former samples include also a (small) fraction of Sa objects and their RCs are of higher spatial resolution (lower bin size) and therefore less efficient in smoothing the non-circular motion caused by bars and spiral arms (ii) the R band is more affected than the I band by random recent episodes of star formation. A conservative estimate of these effects

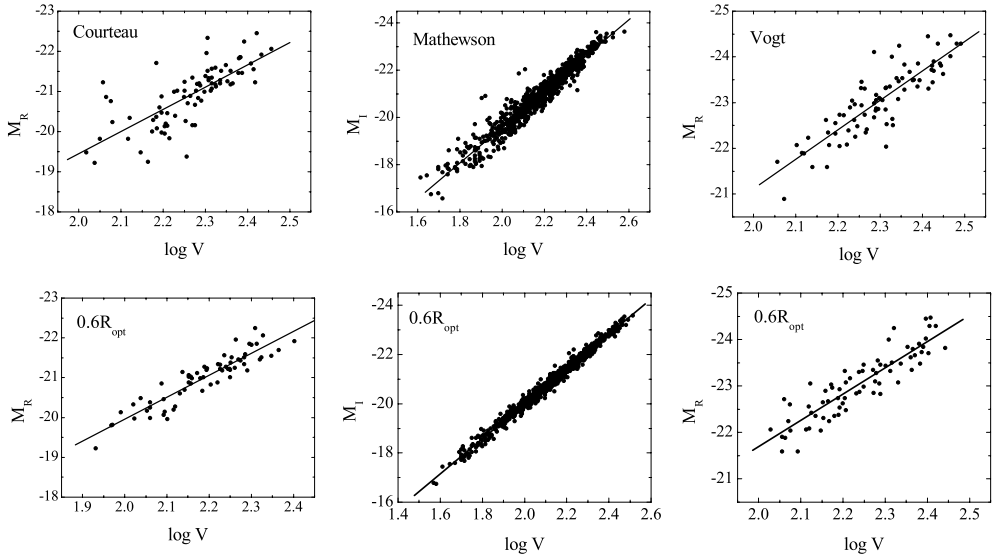

Figure 7. The standard TF relation for all three samples compared with the RTF relation at $R = 0.6R_{opt}$.

is $\sigma_{\rm obs} \geqslant 0.2$, thus the intrinsic scatter of the RTF in the R band $(s_{\rm n}^2 - \sigma_{\rm obs}^2)^{0.5}$ results similar to that found in the I band.

4 RTF: IMPLICATIONS

The marked systematic increase of the slopes of the RTF relationship, as their reference radius $R_{\rm n}$ increases from the galaxy centre to the stellar disc edge, bears very important consequences. First, it excludes, as viable mass models, those in which:

(i) The gravitating mass follows the light distribution, due to a total absence of non-baryonic DM or to DM being distributed similarly to the stellar matter. In both cases, in fact, we do not expect to find any variation of the slopes $a_{\rm n}$ and very trivial variations of the zero-points $b_{\rm n}$ with the reference radius $R_{\rm n}$, contrary to the evidence in Tables A1–A3 and Fig. 4.

(ii) The DM is present but with a luminosity-independent fractional amount inside the optical radius. In this case, in fact, the value of the circular velocity at any reference radius $R_{\rm n}$ will be a {luminosity-independent} fraction of the value at any other reference radius [i.e. $\log V(R_{\rm n}) = k_{\rm nm} + \log V(R_{\rm m})$, $k_{\rm nm}$ independent of luminosity]. As a consequence, the slopes $a_{\rm n}$ in the RTF will be independent of $R_{\rm n}$, while the zero-points $b_{\rm n}$ will change in a characteristic way. It is clear that the evidence in Tables A1–A3 and Fig. 4 contradicts this possibility.

The RTF contains crucial information on the mass distribution in spirals. In Paper II, we will fully recover and test it with theoretical scenarios. Here, instead, we will use a SMM, that includes a bulge, a disc and a halo mass component and it is tunable by means of four free parameters. By matching this model with the slopes of the RTF relation versus reference radii relationship (hereafter SRTF), we derive the *gross* features of the mass distribution in spirals. Let us point out that this method has a clear advantage with respect to the mass modelling based on RCs. In this latter procedure, since the circular velocities have a quite limited variation with radius, physically different mass distributions may reproduce the observations equally well. Here instead, on one side, we will use an observational quantity, the slope of the RTF relation that shows large variation with reference radius; on the other side, physically different mass distributions predict very different slope versus reference radius relationships.

First, without any loss of generality affecting our results, we assume the well-known relationships among the crucial structural properties of spirals:

$$\text{(i)}\ R_{\rm D} = R_1 l^{0.5}, \tag{11a}$$

see PSS, with $\mathrm{l} \equiv 10^{(M_I - M_I{}^{\rm max})/2.5}$ and $M_I^{\rm max} = -23.5$ is the maximum magnitude of our sample, and

$$\text{(ii)}\ M_{\rm D} = M_1 l^{1.3} \tag{11b}$$

(e.g. Shankar et al. 2006, and references therein). Note that the constants R_1 and M_1 will play no role in the following. We will best fit the $a_{\rm n}$ data, i.e. the SRTF relation shown in Fig. 4 with the slopes $a_{\rm SMM}(x)$ we derive from the SMM. In this way, we will fix the free structural mass parameters.

We describe in detail the adopted SMM, the circular velocity is a sum of three contributions generated by the bulge component, taken as a point mass situated in the centre, a Freeman disc and a dark halo, so

$$V^2_{\rm SMM}(x) = G M_{\rm D}/R_{\rm D} \left[f_{\rm d}(x) + \frac{M_{\rm b}}{M_{\rm D}} \frac{1}{(3.2x)} + \frac{M_{\rm halo}}{M_{\rm D}} \frac{1}{3.2} f_{\rm h}(x, \alpha) \right],$$

where $M_{\rm halo}$ is the halo mass inside $R_{\rm opt}$. It is useful to measure $V^2_{\rm SMM}$ in units of GM_1/R_1, and to set it to be equal to 1. The disc component from equations (5) and (11a), (11b) takes the form

$$V^2_{\rm d}(x, l) = l^{0.8} f_{\rm d}(x), \tag{12}$$

with $V^2_{\rm d}(1, 1) = 0.347$.

We set $M_{\rm b}$ as the bulge mass to be equal to a fraction $c_{\rm b}/(3.2 \times 0.347) l^{0.5}$ of the disc mass, with $c_{\rm b}$ being a free parameter of the SMM; the exponent 0.5 in the luminosity dependence is suggested from the bulge-to-disc versus total luminosity trend found for spirals (de Jong 1996). Then, we get

$$V^2_{\rm b}(x) = c_{\rm b} V^2_{\rm d}(1, l) l^{0.5} x^{-1}. \tag{13}$$

The halo velocity contribution follows the profile of equation (6) and at $R_{\rm opt}$ it is set to be equal to $c_{\rm h}/(3.2 \times 0.347) l^{(k_{\rm h}-0.5)}$ times the disc contribution $c_{\rm b}/c_{\rm h}$. Moreover, $k_{\rm h}$ and α are the free parameters of the SMM.

Then, we can write

$$V^2_{\rm SMM}(x, \alpha, l) = \left[c_{\rm b} l^{1.3}/x + l^{0.8} f_{\rm d}(x) + c_{\rm h} l^{(k_{\rm h}-0.5)} f_{\rm h}(x, \alpha) \right], \tag{14}$$

where $f_{\rm d}$ is given by equation (5) and $f_{\rm h}$ is given by equation (6). Note that the simple form of $V_{\rm SMM}$ allows us to get the predicted slope function $a_{\rm SMM}(x)$.

The core radius α is a DM free parameter; however, let us anticipate that, provided this quantity lies between 0.5 and 2 (see Donato, Gentile & Salucci 2004 and Salucci, Walter & Borriello 2003), it does not affect in a relevant way the SMM predictions. Instead the $a_{\rm SMM}(x)$ relationship strongly depends on the values of $c_{\rm h}$, $k_{\rm h}$, $c_{\rm b}$, and therefore they can be estimated with a good precision. We can reproduce the observational $a_{\rm n} = a(R_{\rm n})$ relationship, by means of the SMM (see Fig. 8) with the following best-fitting parameters values: (i) $k_{\rm h} = 0.8 \pm 0.04$, that means less luminous galaxies have larger fraction of DM, (ii) $c_{\rm b} = 0.13 \pm 0.03$, and (iii) $c_{\rm h} = 0.13 \pm 0.06$ that indicates that at $(l, x) = (1, 1)$ (i.e. inside $R_{\rm opt}$), 20 per cent of the mass is in the bulge component, 20 per cent in the halo, while 60 per cent is in the stellar disc (see Figs 9 and 10). The quoted uncertainties are the formal χ^2 fitting uncertainties.

5 DISCUSSION AND CONCLUSIONS

In spirals, at different galactocentric distances measured in units of disc length-scales $jR_{\rm D}(j = 0.2, \ldots, 4)$, there exists a family of

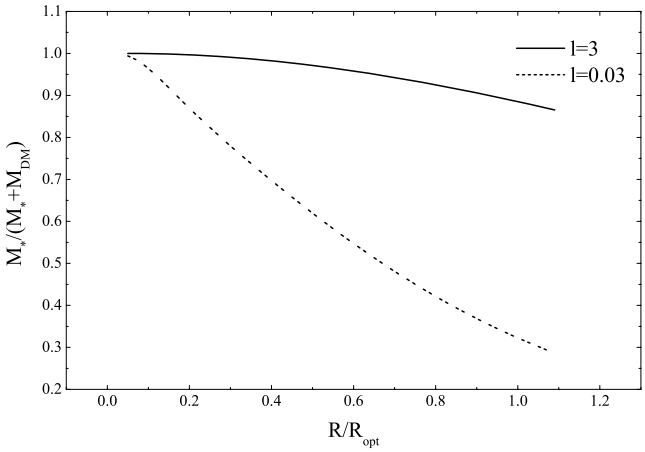

Figure 9. Baryonic mass fraction as a function of normalized radius for high- and low-luminosity objects.

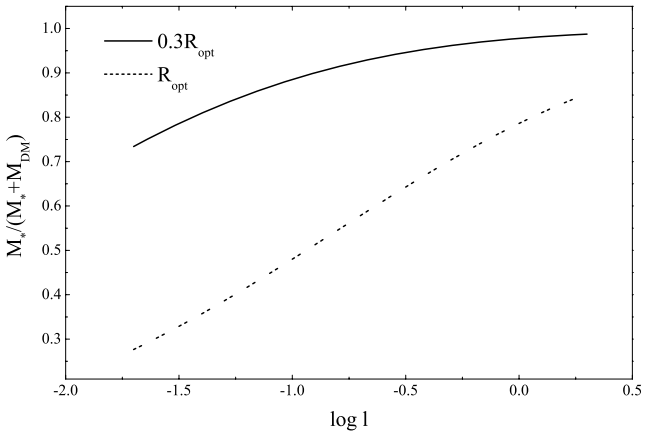

Figure 10. Baryonic mass fraction at two different radii as a function of luminosity.

independent Tully–Fisher-like relationships, $M_{\rm band} = b_j + a_j \log V(R_j)$, that we call the RTF relation, it contains crucial information on the mass distribution in these objects. In fact:

(i) The RTF relationships show large systematic variations in their slopes a_j (between -4 and -8) and a rms scatter generally smaller than that of the standard TF. This rules out the case in which the light follows the gravitating mass, and, in particular, all mass models that imply: (a) an absence of DM, (b) a single mass component (c) the same dark-to-luminous-mass fraction within $jR_{\rm D}$ in all galaxies.

(ii) The slopes a_j decrease monotonically with R_j, which implies the presence of a non-luminous mass component whose dynamical importance, with respect to the stellar disc, increases with radius.

(iii) The existence of the RTF and the features of the slope versus R_j can be well reproduced by means of a three components mass model that includes a dark halo, with $1.6\,R_{\rm D} < R_{\rm c} < 6.4R_{\rm D}$, and mass $M_{\rm halo}(R_{\rm opt}) \propto l^{0.8}$, a central bulge with $M_{\rm bulge} \propto l^{1.8}$, an exponential thin disc of mass $M_{\rm d} \propto l^{1.3}$ with, at $10^{11}\,{\rm L}_{B,\odot}$, 80 per cent of the mass inside $R_{\rm opt}$ in the stellar form.

Let us also note that we have produced a qualitatively new evidence for the presence of a luminosity-dependent mass discrepancy in spirals, different from that obtained from the non-Keplerian shapes of the RCs. While the latter originates from a failure, we do not observe the Keplerian fall-off of the circular velocities at the disc edge, and therefore we must postulate a new component, here, we provide a *positive* evidence for the existence of such a dark component; we *detect* radial change of the slope and the scatter of existing relations between observables that positively indicates the presence of a more diffuse dark component.

The small scatter of the RTF implies that, in spirals, at any radius, the luminosity is an extremely efficient statistical estimator of the *rotation* velocity. This, since otherwise the strong correlation between luminosity and rotation velocities would be an unacceptably fortuitous coincidence, strongly supports in contrast with a different claim (Hayashi) that in spirals this velocity coincides with the *circular* velocity, i.e. with the centrifugal equilibrium velocities $V_{\rm c}$ associated with the central galaxy gravitational potential Φ, $V_{\rm c} = (-R\,{\rm d}\Phi/{\rm d}R)^{1/2}$).

Finally, let us stress that any model of formation of spiral galaxies must be able to produce (e.g. in the I band) a M_I versus $\log V(2R_{\rm D})$ relationship with a slope of 7 ± 0.1 and an intrinsic scatter of $\leqslant$0.15 mag.

ACKNOWLEDGMENTS

We thank S. Courteau and N. Vogt for kindly provided data. We also thank Gianfranco Gentile for helping us with preparation of this paper. We want to thank the anonymous referee for detailed comments that much improved the final version of this paper.

REFERENCES

Aaronson M. et al., 1982, ApJS, 50, 241
Courteau S., 1996, ApJS, 103, 363
Courteau S., 1997, AJ, 114, 2402
de Jong R. S., 1996, A&A, 313, 45
Donato F., Gentile G., Salucci P., 2004, MNRAS, 353, L17
Freeman K. C., 1970, ApJ, 160, 811
Gentile G., Salucci P., Klein U., Vergani D., Kalberla P., 2004, MNRAS, 351, 903
Mathewson D. S., Ford V. L., Buchhorn M., 1992a, ApJS, 81, 413
Persic M., Salucci P., 1988, MNRAS, 234, 131
Persic M., Salucci P., 1995, ApJS, 99, 501 (PS95)
Persic M., Salucci P., Stel F., 1996, MNRAS, 281, 27 (PSS)
Pierce M., Tully R. B., 1988, ApJ, 330, 579
Pierce M., Tully R. B., 1992, ApJ, 387, 47
Rhee M. H., 1996, PhD thesis, Univ. Groningen
Salucci P., Gentile G., 2006, Phys. Rev. Lett. D, 73, 128501
Salucci P., Frenk C. S., Persic M., 1993, MNRAS, 262, 392
Salucci P., Walter F., Borriello A., 2003, A&A, 409, 53
Shankar F., Lapi A., Salucci P., De Zotti G., Danese L., 2006, ApJ, 643, 14
Strauss M. A., Willick J. A., 1995, Phys. Rep., 261, 271
Tully R. B., Fisher J. R., 1977, A&A, 54, 661
Vogt N. P., Haynes M. P., Herter T., Giovanelli R., 2004, AJ, 127, 3273

APPENDIX A:

In this appendix, we present Tables-A1–A6 and Figs A1 and A2 related to the results described in the previous sections concerning Samples 2 and 3.

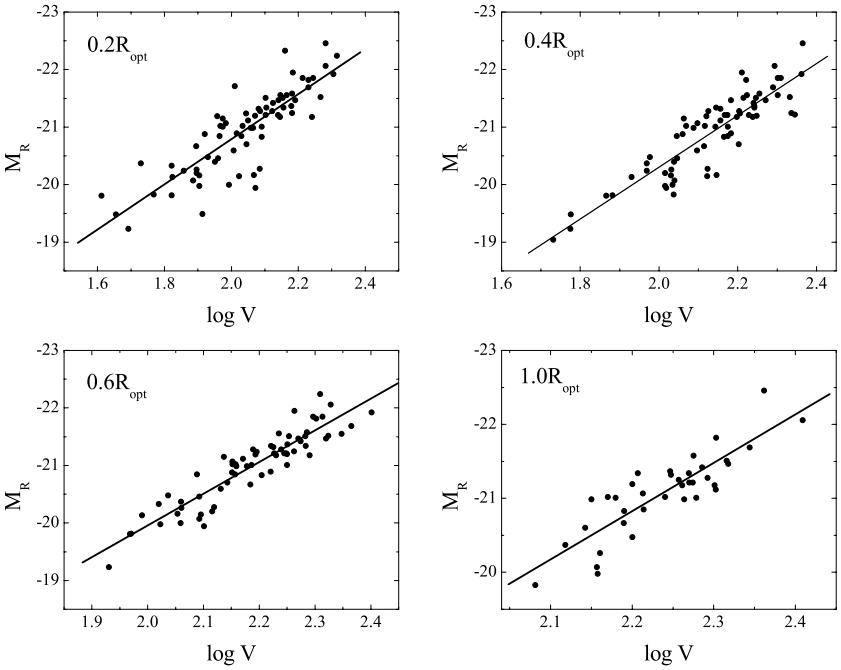

Figure A1. The RTF relation for the Courteau sample.

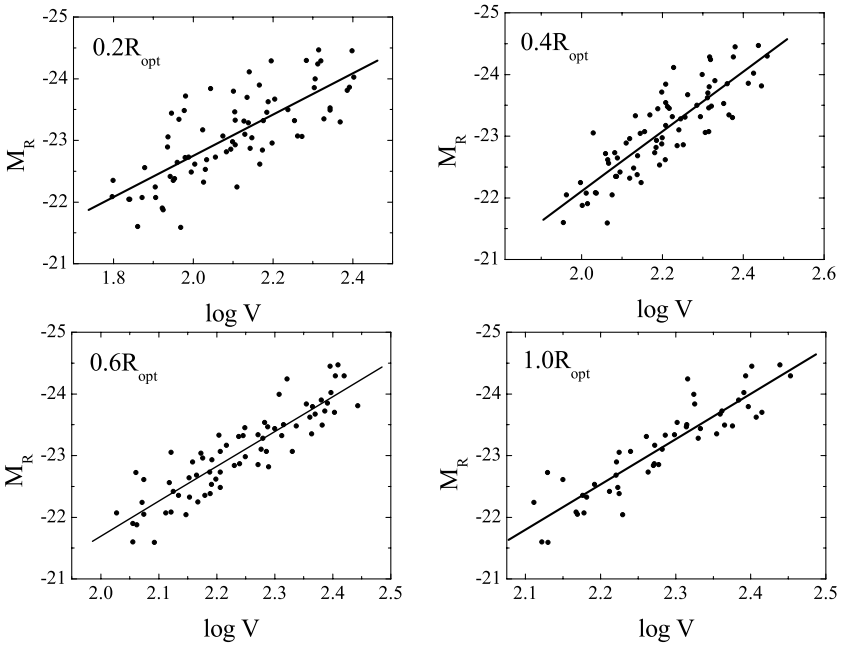

Figure A2. The RTF relation for the Vogt sample.

Table A1. Parameters of the RTF relation at different radii for the Mathewson sample.

R/R_{opt}	Zero-point	Error	Slope	Error	SD	N
0.2	−11.78	0.103	−4.77	0.054	0.366	739
0.4	−8.241	0.068	−6.141	0.033	0.185	786
0.6	−5.787	0.063	−7.102	0.029	0.146	794
0.8	−4.22	0.09	−7.718	0.042	0.17	657
1.0	−3.034	0.146	−8.197	0.067	0.208	447
1.2	−1.979	0.261	−8.639	0.118	0.253	226

Notes. Column 1 – the isophotal radius; Column 2 – intercept value b_n; Column 3 – the standard error of b_n; Column 4 – the slope a_n; Column 5 – the standard error of a_n; Column 6 – the scatter; Columns 7 – the number of observational points.

Table A2. Parameters of the RTF relation at different radii for the Courteau sample.

R/R_{opt}	Zero-point	Error	Slope	Error	SD	N
0.03	−18.217	0.287	−1.8	0.189	0.516	75
0.09	−15.615	0.39	−2.878	0.209	0.381	74
0.16	−14.355	0.495	−3.336	0.249	0.388	75
0.22	−13.379	0.55	−3.707	0.27	0.397	76
0.28	−12.155	0.741	−4.194	0.355	0.465	79
0.34	−11.7	0.613	−4.374	0.291	0.361	74
0.41	−11.11	0.617	−4.586	0.289	0.338	72
0.47	−9.962	0.674	−5.086	0.31	0.295	68
0.53	−9.114	0.699	−5.445	0.321	0.296	71
0.59	−8.919	0.733	−5.519	0.334	0.293	68
0.66	−8.623	0.752	−5.61	0.341	0.279	65
0.72	−8.351	0.625	−5.737	0.284	0.255	63
0.78	−8.172	0.763	−5.799	0.345	0.274	61
0.84	−7.329	1.0	−6.152	0.456	0.32	53
0.91	−6.372	1.0	−6.58	0.449	0.286	44
0.97	−7.573	1.54	−6.042	0.688	0.31	37
1.03	−7.728	1.993	−5.984	0.888	0.311	25
1.09	−9.265	2.254	−5.307	1.0	0.212	14
1.16	−6.853	1.767	−6.35	0.789	0.281	15

Table A3. Parameters of the RTF relation at different radii for the Vogt sample.

R/R_{opt}	Zero-point	Error	Slope	Error	SD	N
0.09	−19.351	0.526	−1.992	0.278	0.55	78
0.16	−18.118	0.64	−2.456	0.316	0.528	78
0.22	−16.142	0.714	−3.309	0.339	0.472	76
0.28	−14.787	0.728	−3.869	0.338	0.43	77
0.34	−13.583	0.73	−4.365	0.334	0.394	77
0.41	−12.646	0.78	−4.747	0.354	0.386	77
0.47	−11.746	0.784	−5.112	0.353	0.365	77
0.53	−11.342	0.805	−5.264	0.361	0.361	75
0.59	−10.698	0.778	−5.51	0.347	0.327	72
0.66	−9.804	0.77	−5.885	0.341	0.309	71
0.72	−9.244	0.83	−6.125	0.368	0.318	70
0.78	−9.227	0.936	−6.104	0.414	0.341	68
0.84	−7.873	0.906	−6.7	0.4	0.304	60
0.91	−7.435	1.057	−6.893	0.466	0.334	58
0.97	−6.377	1.153	−7.343	0.505	0.323	50
1.03	−8.398	1.414	−6.435	0.62	0.345	41
1.09	−7.953	1.377	−6.628	0.599	0.301	35
1.16	−8.683	1.38	−6.947	0.622	0.228	24
1.22	−9.616	1.444	−6.842	0.714	0.275	23
1.28	−7.394	2.467	−6.834	1.072	0.347	16

Table A4. Parameters of the standard Tully–Fisher relation for three samples.

Data	Zero-point	Error	Slope	Error	SD	N
Mathewson	−4.455	0.15	−7.57	0.069	0.327	841
Courteau	−8.398	1.26	−5.526	0.556	0.495	81
Vogt et al.	−8.277	0.997	−6.423	0.433	0.389	79

Table A5. Names of galaxies from the Courteau sample.

UGC 10096	UGC 10196	UGC 10210	UGC 10224
UGC 1053	UGC 10545	UGC 10560	UGC 10655
UGC 10706	UGC 10721	UGC 10815	UGC 11085
UGC 11373	UGC 1152	UGC 11810	UGC 12122
UGC 12172	UGC 12200	UGC 12294	UGC 12296
UGC 12304	UGC 12325	UGC 12354	UGC 12598
UGC 12666	UGC 1426	UGC 1437	UGC 1531
UGC 1536	UGC 1706	UGC 1812	UGC 195
UGC 2185	UGC 2223	UGC 2405	UGC 2628
UGC 3049	UGC 3103	UGC 3248	UGC 3269
UGC 3270	UGC 3291	UGC 3410	UGC 346
UGC 3652	UGC 3741	UGC 3834	UGC 3944
UGC 4232	UGC 4299	UGC 4326	UGC 4419
UGC 4580	UGC 4779	UGC 4996	UGC 5102
UGC 540	UGC 562	UGC 565	UGC 5995
UGC 6544	UGC 6692	UGC 673	UGC 7082
UGC 732	UGC 7549	UGC 7749	UGC 7810
UGC 7823	UGC 783	UGC 784	UGC 8054
UGC 8118	UGC 8707	UGC 8749	UGC 8809
UGC 890	UGC 9019	UGC 9366	UGC 9479
UGC 9598	UGC 9745	UGC 9753	UGC 9866
UGC 9973			

Table A6. Names of galaxies from the Vogt sample.

UGC 927	UGC 944	UGC 1033	UGC 1094
UGC 1437	UGC 1456	UGC 1459	UGC 2405
UGC 2414	UGC 2426	UGC 2518	UGC 2618
UGC 2640	UGC 2655	UGC 2659	UGC 2700
UGC 3236	UGC 3270	UGC 3279	UGC 3289
UGC 3291	UGC 3783	UGC 4275	UGC 4287
UGC 4324	UGC 4607	UGC 4655	UGC 4895
UGC 4941	UGC 5166	UGC 5656	UGC 6246
UGC 6437	UGC 6551	UGC 6556	UGC 6559
UGC 6718	UGC 6911	UGC 7845	UGC 8004
UGC 8013	UGC 8017	UGC 8108	UGC 8118
UGC 8140	UGC 8220	UGC 8244	UGC 8460
UGC 8705	UGC 10190	UGC 10195	UGC 10459
UGC 10469	UGC 10485	UGC 10550	UGC 10981
UGC 11455	UGC 11579	UGC 12678	UGC 12755
UGC 12792	UGC 150059	UGC 180598	UGC 210529
UGC 210559	UGC 210629	UGC 210634	UGC 210643
UGC 210789	UGC 211029	UGC 220864	UGC 221174
UGC 221206	UGC 251400	UGC 260640	UGC 260659
UGC 330781	UGC 330923	UGC 330925	UGC 330996
UGC 331021			

This paper has been typeset from a TEX/LATEX file prepared by the author.